Title: Intracranial Paragangliomas versus Schwannomas: Role of Dynamic Susceptibility Contrast Perfusion and Diffusion MRI

Running title: Paragangliomas vs schwannomas: Utility of DWI and DSC-MRI

Authors:

Yoshiaki Ota, MD[1], Eric Liao, MD [1], Aristides A. Capizzano, MD [1], Akira Baba, MD, PhD [1], Ryo Kurokawa, MD, PhD [1], Mariko Kurokawa, MD [1], Ashok Srinivasan, MD [1]

[1]Division of Neuroradiology, Department of Radiology, University of Michigan, 1500 E Medical Center Dr, UH B2, Ann Arbor, MI 48109, USA

Keywords: DWI; DSC perfusion MRI; paraganglioma; NF2; vestibular schwannoma

Corresponding author: Yoshiaki Ota

1500 E Medical Center Dr, UH B2, Ann Arbor, MI 48109, USA

Phone: 7348825904 FAX number: 7346159800

Email address: yoshiako@med.umich.edu

Funding: There was no funding or grant support for this study.

Abstract:

Background and Purpose: Differentiating paragangliomas from schwannomas and distinguishing sporadic from neurofibromatosis type 2 (NF 2)-related schwannomas is challenging but clinically important. This study aimed to assess the utility of dynamic susceptibility contrast perfusion MRI

(DSC-MRI) and diffusion-weighted imaging (DWI) in discriminating infratentorial extra-axial schwannomas from paragangliomas and NF2-related schwannomas.

Methods: This retrospective study included 41 patients diagnosed with paragangliomas, sporadic schwannomas, and NF2-related schwannomas in the infratentorial extra-axial space between April 2013 and August 2021. All cases had pretreatment DSC-MRI and DWI. Normalized mean apparent diffusion coefficient (nADCmean), normalized relative cerebral blood volume (nrCBV), and normalized relative cerebral blood flow (nrCBF) were compared between paragangliomas and schwannomas and between sporadic and NF2-related schwannomas as appropriate.

Results: nrCBV and nrCBF were significantly higher in paragangliomas than in sporadic/NF2-related schwannomas (nrCBV: median 11.5 vs 1.14/3.74; p< .001 and .004, nrCBF: median 7.43 vs 1.13/2.85; p< .001 and .007, respectively), while nADCmean were not. The corresponding diagnostic performances were area under the curves (AUCs) of 0.99/0.92 and 1.0/0.90 with cutoffs of 2.56/4.22 and 1.94/3.36, respectively. nADCmean were lower, and nrCBV and nrCBF were higher in NF2-related than in sporadic schwannomas (nADCmean: median 1.23 vs 1.58, nrCBV: median 3.74 vs 1.14, nrCBF: median 2.85 vs 1.13; all p< .001), and the corresponding diagnostic performances were AUCs of 0.93, 0.91, and 0.95 with cutoffs of 1.37, 2.63, and 2.48, respectively.

Conclusions: DSC-MRI and DWI both can aid in differentiating paragangliomas from schwannomas and sporadic from NF2-related schwannomas.

Introduction:

Infratentorial extra-axial tumors are common and encompass a broad range of tumors including paragangliomas and schwannomas.[1,2] These tumors can demonstrate classic features on conventional imaging. Paragangliomas can be visualized on MRI as heterogeneously enhancing tumors with flow voids or “salt-and pepper” signal appearance,[3-5] while schwannomas can present as heterogeneously enhancing tumors with cystic change or dumbbell-shaped appearance.[6,7]

However, these imaging findings are not specific and can overlap between paragangliomas and schwannomas. As for anatomic location, infratentorial extra-axial paragangliomas and schwannomas are mainly observed in the jugular foramen and cerebellopontine cisterns, respectively, but can involve both anatomic areas[5,7] and also involve the prepontine cistern.[7,8] Definitive diagnosis relies on pathological confirmation such as biopsy, which is invasive and technically challenging in the above locations, where multiple nerves and vascular structures course. Furthermore, schwannomas can be linked to neurofibromatosis type 2 (NF2), which commonly involves the bilateral vestibular nerves. NF2 can be diagnosed with the Manchester criteria, including bilateral vestibular schwannomas, family history of NF2, and other extra-axial tumors such as meningiomas and ependymomas.[9,10] However, it is known that half of NF2 cases do not carry a family history of NF2 and unilateral vestibular schwannomas or other cranial nerve schwannomas can be observed in NF2,[10] which makes diagnosis of NF2 challenging. NF2-related schwannomas can display rapid growth,[9,10] so early NF2 detection is important.

Recently, diffusion-weighted imaging (DWI) and perfusion MRI have been utilized for tumor differentiation, gene mutation detection, and treatment monitoring by assessing internal microstructure and vascularity of the tumors.[11-16] Paragangliomas are known to be hypervascular tumors while schwannomas show a relatively slow enhancement pattern compared to paragangliomas.[12] Also, there are differences in internal microstructure between the two tumors and even between sporadic and NF2-related schwannomas.[3,10,17] There have been some studies assessing the differentiation of paragangliomas and schwannomas using dynamic contrast-enhanced MRI,[12,18] but assessment of dynamic susceptibility contrast perfusion MRI (DSC-MRI) and DWI for the two tumor types and NF2 gene mutation status of infratentorial extra-axial schwannomas has not been fully elucidated.

In this study, we aimed to assess the utility of DWI and DSC-MRI for differentiation of intracranial paragangliomas and schwannomas and discrimination of intracranial schwannoma NF2 gene mutation status.

Methods:

Study population

Our institutional review board approved this retrospective single-center study and waived the requirement for informed consent. Data were acquired in compliance with all applicable Health Insurance Portability and Accountability Act regulations. We retrospectively reviewed clinical records and imaging from 409 patients with pathologically confirmed intracranial paragangliomas and schwannomas at our institution between April 2013 and August 2021. We excluded patients who did not have pre-treatment MRI including dynamic susceptibility contrast perfusion MRI and DWI (n = 350), or cases where pre-treatment MRI imaging quality was too poor to evaluate (n = 14). In addition, we excluded bilateral 4 vestibular schwannomas (n=4) because the Manchester criteria includes bilateral vestibular tumors, which does not need imaging differential diagnosis. In total, 41 patients (male:18, female:23; age 7-74 years) comprising a total of 12 intracranial paragangliomas and 29 intracranial schwannomas were included.

Among patients with schwannomas, there were 19 patients with sporadic schwannomas, and 10 patients with NF2-related schwannomas. In the sporadic schwannomas group, all patients had pathologically diagnosed schwannoma and did not meet the Manchester criteria for NF2[10]. Two patients underwent NF2 mutational analysis using blood with negative results of germline NF2 mutation or LZTR1 and SMARCB1. In the NF2-related schwannomas group, all patients had pathologically diagnosed schwannomas and met the Manchester criteria. Eight patients had unilateral vestibular schwannomas and intracranial meningiomas, and 4 out of 8 patients have family history of NF2. Each of the two remaining patients had a trigeminal schwannoma or a jugular

foramen schwannoma, multiple intracranial meningiomas, and family history of NF2. Eight patients underwent NF2 mutational analysis with positive results of germline NF2 mutation using blood samples.

MRI acquisition

All MRI examinations were performed using 1.5T or 3T (Ingenia; Philips, Eindhoven, MAGNETOM Vida; Siemens, Munich) using a 16-channel neurovascular coil. Acquired sequences included axial T2WI, axial T1WI, axial fluid-attenuated inversion recovery (FLAIR), and axial pre- and postcontrast 3D-T1WI. DWI sequences using echo-planar imaging were performed with b-values of 0 and 1000 s/mm^2 and the following parameters: repetition time range: 5000–8700 ms; echo time: range: 58–106 ms; number of excitations: 1; slice thickness/gap: 4/0-1 mm; field of view: 240 mm x 240 mm; pixel size: 1.5 × 1.5 mm, and 3 diffusion directions.

DSC-MRI was performed following an intravenous bolus of total 20mL of gadobenate dimeglumine (Multihance, Bracco diagnostics, Singen, Germany) using a power injector with a flow rate of 5.0 mL/s through a peripheral arm vein, followed by a 20 mL saline flush. A 5mL of the contrast 5 minutes prior to the dynamic perfusion scan. The parameters of fast field echo T2*-weighted DSC-MRI sequence were as follows: plane = axial; repetition time = 1500–1920ms; echo time = 30–50 ms; number of excitations = 1; slice thickness = 4–4.4mm; slice increment = 5–5.2mm; field of view = 220–240mm; matrix, 128 × 128–144 × 144; dynamic measurements, 40; temporal resolution, 1.5sec; total acquisition time, 1min 4.5sec

Patient demographics

Patient demographics such as age at diagnosis, sex for each patient, histological diagnoses, and NF2 gene mutation status were reviewed from the medical records.

Imaging processing and analysis

Two board-certified radiologists with 7 (Y.O.) and 10 (E.L.) years of experience independently reviewed conventional imaging findings and performed DWI and DSC-MRI analysis. The clinical information, histopathological results, and imaging results were blinded to the two readers.

Conventional imaging analysis

Maximal diameter of the tumors was evaluated on post-contrast axial fat saturated T1-weighted images. Cystic or necrotic changes were recorded as a binary variable using a combination of axial T1WI, T2WI, FLAIR, and pre- and post-contrast T1WI. As well, the enhancement pattern (homogenous versus heterogenous) was evaluated on pre- and postcontrast T1WI.

DWI analysis

A single freehand region of interest (ROI) was manually drawn on the axial postcontrast 3D-T1WI at the slice of greatest axial diameter, encompassing areas of solid enhancement and taking care to avoid cystic or necrotic areas as well as adjacent vasculature. To avoid volume averaging artifact, the peripheral 2 mm of the lesions was excluded. Apparent diffusion coefficient (ADC) maps were constructed using commercially available software (Olea Sphere, Version 3.0; Olea Medical). The corresponding ROIs were again contoured on the ADC map with reference to axial postcontrast 3D-T1WI, and adjusted to exclude geometric artifact as needed. As an internal control, a ROI was placed within the medulla oblangata. A normalized mean ADC ratio (nADCmean) was calculated by dividing each lesion's ADC value by the ADC value of medulla oblongata to adjust for the variation of scanners and magnetic field strengths.

DSC-MRI analysis

DSC-MRI analysis also was performed using Olea Sphere. The arterial input function (AIF) was automatically computed. While this process was automated, the corresponding attenuation time curves that demonstrated a rapid increase in attenuation with sharp peaks were used for analysis. Relative cerebral blood volume (rCBV) and relative cerebral blood flow (rCBF) maps were generated with the use of voxel-wise division of the area under the concentration-time curve by the area under the AIF. ROIs were placed on the solid components of tumors with reference to axial postcontrast T1WI, following the same method used for ADC analysis. Additionally, 2 ROIs were placed on the normal-appearing bilateral middle cerebellar peduncles to control for variation in magnet type and

field strength. Normalized rCBF (nrCBF) and normalized rCBV (nrCBV) were calculated by dividing rCBV and rCBF of the tumors by the corresponding averaged values of the reference. Representative cases of intracranial paraganglioma, intracranial sporadic schwannoma, and intracranial NF2-related schwannoma are demonstrated in Fig. 1, Fig. 2, and Fig. 3, respectively.

Statistical analysis

Inter-reader agreements for conventional imaging variables such as cystic or necrotic changes and enhancement patterns and numerical variables such as nADCmean, nrCBV, and nrCBF were assessed using the kappa coefficient and the intraclass correlation coefficient, respectively. The result of a board-certified neuroradiologist with 7 years of experience (Y.O.) was applied. The conventional imaging variables such as cystic or necrotic change and enhancement pattern (homogeneous/heterogeneous pattern) were compared by Fisher exact test and maximum axial diameter was compared among paragangliomas, sporadic and NF2-related schwannomas. nADCmean and DSC-MRI parameters (nrCBV and nrCBF) were compared among paragangliomas, sporadic, and NF2-related schwannomas by Kruskal–Wallis H test and post hoc test with Bonferroni correction. Following Kruskal-Wallis H test, each pair of tumor types (paragangliomas versus sporadic schwannomas, paragangliomas versus NF2-related schwannomas, and sporadic vs NF2-related schwannomas) were compared. The numerical variables were described as median (interquartile range). For statistically significant parameters, receiver operating characteristic (ROC) analysis was performed with the optimal cutoff values which were determined to maximize the Youden index (sensitivity + specificity - 1). All statistical calculations were conducted using R software (version 4.1.1; R Core Team, Vienna, Austria). Variables with P-values of < .05 were considered statistically significant.

Results:

Inter-reader agreement

The inter-reader agreements for conventional imaging variables such as cystic or necrotic change and enhancement pattern and numerical variables such as nADCmean, nrCBV, and nrCBF are summarized in Table 4. The kappa coefficient and intraclass correlation coefficient were moderate to good (kappa= 0.566-0.609) and almost perfect (intraclass correlation coefficient= 0.923-0.950), respectively.

Patient demographics

Patients' demographics are summarized in Table 1. There were 12 intracranial paragangliomas (6 men, 6 women; median age 31 years [22-48]), 19 sporadic schwannomas (11 men, 8 women; median age 50 years [43-58]), and 10 NF2-related schwannomas (1 men, 9 women; median age 21 years [16-53]). Intracranial paragangliomas were located in the jugular foramen (12/12), sporadic schwannomas in the cerebellopontine angle (vestibular nerve) (11/19), prepontine cistern (trigeminal nerve) (3/19), and jugular foramen (glossopharyngeal nerve, vagal nerve, or accessory nerve) (5/19), and NF2-related schwannomas were located in the cerebellopontine angle (8/10), prepontine cistern (1/10), and jugular foramen (1/10).

Conventional imaging

The conventional imaging features are summarized in Table 2. Cystic or necrotic change and homogeneous enhancement were seen in 9/12 and 2/12 cases of infratentorial extra-axial paraganglioma, in 12/19 and 6/19 cases of sporadic schwannomas, and in 7/10 and 5/10 cases of NF2-related schwannomas, respectively. There were no significant differences in conventional MRI findings among intracranial paragangliomas, sporadic schwannomas, and NF2-related schwannomas.

DWI and DSC-MRI analysis

Table 3 and Figure 4 represent the results of the Kruskal–Wallis H test and post hoc test with Bonferroni correction among intracranial paragangliomas, intracranial sporadic, and intracranial NF2-related schwannomas, as well as the results of each pair of tumor types (paragangliomas versus sporadic schwannomas, paragangliomas versus NF2-related schwannomas, and sporadic vs NF2-related schwannomas).

Intracranial paraganglioma vs. intracranial sporadic or NF2-related schwannomas

nADCmean was not significantly different between intracranial paragangliomas and sporadic or NF2-related schwannomas (paraganglioma vs sporadic or NF2-related schwannoma: median 1.49 [1.19-1.58] vs 1.58 [1.45-1.80] or 1.23 [1.17-1.34]; p= .26 and .29, respectively). nrCBV and nrCBF were higher in intracranial paragangliomas than in intracranial sporadic or NF2-related schwannomas (nrCBV median 11.5 [6.24-13.6] vs 1.14 [0.94-1.34] or 3.74 [2.86-4.84]; p < .001 and p= .004, respectively; nrCBF median 7.43 [4.30-11.4] vs 1.13 [1.02-1.46] or 2.85 [2.51-4.04]; p < .001 and p= .007, respectively). In ROC analysis, nrCBV and nrCBF between intracranial paragangliomas and intracranial sporadic schwannomas showed 0.99 and 1.0 area under the curves (AUCs), 0.94 and 1.0 sensitivity, 1.0 and 1.0 specificity, 1.0 and 1.0 positive predictive value (PPV), 0.92 and 1.0 negative predictive values (NPV), and 0.96 and 1.0 accuracy, with cut-off values of 2.56 and 1.94, respectively. nrCBV and nrCBF between intracranial paragangliomas and intracranial NF2-related schwannomas showed 0.92 and 0.9 AUCs, 0.70 and 0.70 sensitivity, 1.0 and 1.0 specificity, 1.0 and 1.0 PPV, 0.77 and 0.77 NPV, and 0.85 and 0.85 accuracy with cut-off values of 4.22 and 3.36, respectively.

Intracranial sporadic vs. NF2-related schwannomas

nADCmean was significantly higher in sporadic than in NF2-related schwannomas (sporadic vs NF2-related schwannoma: median 1.58 [1.45-1.80] vs 1.23 [1.17-1.34]; p< .001). nrCBV and nrCBF

were lower in sporadic than in NF2-related schwannomas (nrCBV: median 1.14 [0.94-1.35] vs 3.74 [2.90-4.84]; p < .001, nrCBF: median 1.13 [1.02-1.46] vs 2.85 [2.51-4.04]; p < .001). In ROC analysis, nADCmean, nrCBV, and nrCBF between intracranial sporadic and NF2-related schwannomas showed 0.93, 0.91 and 0.95 AUCs, 0.90, 0.90, and 0.80 sensitivity, 0.95, 0.94, and 1.0 specificity, 0.90, 0.90, and 1.0 PPV, 0.95, 0.94, and 0.90 NPV, and 0.93, 0.93, and 0.93 accuracy, with cut-off values of

Discussion:

This study aimed to test the utility of DWI and DSC-MRI to differentiate intracranial paragangliomas, intracranial sporadic schwannomas, and NF2-related schwannomas. nADCmean showed a significant difference between intracranial sporadic and NF2-related schwannomas with a diagnostic performance of 0.93 AUC, though was not significantly different when comparing intracranial paragangliomas vs. intracranial sporadic or NF2-related schwannomas. nrCBV and nrCBF differentiated intracranial paragangliomas from intracranial sporadic and NF2-related schwannomas and discriminated intracranial sporadic from NF2-related schwannomas, with diagnostic performances of 0.99 and 1.0 AUCs and 0.91 and 0.95 AUCs, respectively.

Regarding DWI analysis, there was a significant difference in nADCmean between sporadic and NF2-related schwannomas. A pathological study suggested foci of hypercellularity in NF2-related schwannomas as compared to sporadic schwannomas, without significant difference in presence of cystic change.[17] The pathological difference in cellularity could be a factor resulting in lower ADC values in NF2-related schwannomas, as one prior study suggested in vestibular schwannomas.[19] There was no significant difference in ADC values between intracranial paragangliomas and intracranial sporadic or NF2-related schwannoma. Insignificant differences in ADC values between paragangliomas and schwannomas were previously reported in prior studies using head and neck paragangliomas and schwannomas, which imply that this could be due to the fact that both

paragangliomas and schwannomas show a variety of histological patterns that can result in heterogeneity of ADC values.[12] The difference of ADC values between paragangliomas and NF2-related schwannomas has not been discussed in prior studies yet, but based on our result, ADC values may not a reliable marker to distinguish between them. We normalized ADC values by medulla oblongata, which is less commonly affected by chronic microvascular disease or direct tumor invasion.[11]

Regarding DSC-MRI, nrCBV and nrCBF were higher in intracranial paragangliomas than in intracranial sporadic or NF2-related schwannomas. DSC-MRI technique can provide physiologic information regarding tumor's microvasculature and vascular permeability, and CBV and CBF are the most commonly used parameters for brain tumor differentiation, tumor grading, and treatment response assessment.[20-22] However, this technique has not been often utilized for intracranial extra-axial tumors.[13,14] Paragangliomas are hypervascular tumors with prominent vascular structures, and prior studies using dynamic contrast-enhanced perfusion MRI (DCE-MRI) showed that fractional plasma volume, which represents tumor's microvascularity, was higher in paragangliomas than in schwannomas.[12,18] Our result suggests that CBV and CBF can also be promising parameters to differentiate paragangliomas and schwannomas. Interestingly, NF2-related schwannomas showed higher CBV and CBF than sporadic schwannomas with diagnostic performance of 0.91 and 0.95 AUCs in this study. Prior studies have shown that vascular permeability can be related to schwannoma growth,[23] and NF2-related schwannomas can grow faster than sporadic schwannomas.[24] DSC-MRI technique can be more helpful to differentiate sporadic from NF2-related schwannomas than DCE-MRI technique, which revealed diagnostic performance of 0.90 AUC by permeability parameters of Ktrans and Ve in prior studies.[18] Accurate diagnosis for head and neck tumors is highly important because each tumor has different treatment strategies. For normalization of rCBV and rCBF, we applied the averaged values of 2 regions of normal-appearing bilateral middle cerebellar peduncles,

where rCBV and rCBF appeared stable in the middle cerebellar peduncle but variable in the medulla oblongata. Applying the averaged values is believed to make our result robust.

In this study, DSC-MRI parameters distinguished intracranial paragangliomas and schwannomas with promising diagnostic performances. When conventional imaging is indecisive for differentiation of the two tumors and DCE-MRI cannot be technically performed, adding DSC-MRI can be helpful for tumor differentiation. As well, intracranial sporadic and NF2-related schwannomas were distinguished by DWI and DSC-MRI parameters. When NF2 gene mutation status is uncertain from a patient's clinical manifestations and conventional imaging findings, adding DWI and DSC-MRI to the head and neck protocol can be beneficial for distinguishing NF2-related from sporadic schwannomas, and thus assist in the appropriate clinical workup and treatment.

There were several limitations in this study. First, this was a single institutional retrospective study including a relatively small population. Further studies with a larger sample size would be necessary to confirm our results. Second, a combination of 1.5 T and 3 T scanners were used, which may add heterogeneity to the calculated ADC and DSC-MRI parameters. However, utilizing normalized values for DWI and DSC-MRI analysis to control for variation between different magnetic field strengths is believed to make the results of ADC, rCBV, and rCBF robust. Third, DSC-MRI can have susceptibility artifacts at tissue interfaces or skull base area, which can obscure ROI placement. However, we believed that we successfully managed susceptibility artifact by excluding the peripheral 2mm of the tumors or adjusting the ROIs when this was observed. Finally, genetic tests were not performed for most of the patients with intracranial sporadic schwannomas. However, these patients were not suspected to have germline NF2 mutation given the Manchester criteria, and did not show any evidence of NF2-related manifestations at follow-up.

In conclusion, both DWI and DSC-MRI can provide promising biomarkers for differentiation between intracranial paragangliomas and schwannomas and for distinguishing sporadic and NF2-related schwannomas, and can be beneficial for a proper clinical assessment.

Acknowledgements and Disclosure: The authors declare no conflicts of interest.

References:

1. Vogl TJ, Bisdas S. Differential diagnosis of jugular foramen lesions. Skull Base 2009;19:3-16.

2. Smirniotopoulos JG, Yue NC, Rushing EJ. Cerebellopontine angle masses: radiologic-pathologic correlation. Radiographics 1993;13:1131-47.

3. Williams MD. Paragangliomas of the head and neck: an overview from diagnosis to genetics. Head Neck Pathol 2017;11:278-87.

4. Withey SJ, Perrio S, Christodoulou D, et al. Imaging features of succinate dehydrogenase-deficient pheochromocytoma-paraganglioma syndromes. Radiographics 2019;39:1393-410

5. Woolen S, Gemmete JJ. Paragangliomas of the head and neck. Neuroimaging Clin N Am 2016;26:259-78

6. Biswas D, Marnane CN, Mal R, et al. Extracranial head and neck schwannomas--a 10-year review. Auris Nasus Larynx 2007;34:353-9

7. Skolnik AD, Loevner LA, Sampathu DM, et al. Cranial nerve schwannomas: diagnostic imaging approach Radiographics 2016;36:1463-77

8. Prajsnar A, Balak N, Walter GF, et al. Recurrent paraganglioma of Meckel's cave: Case report and a review of anatomic origin of paragangliomas. Surg Neurol Int 2011;2:45

9. Evans GR, Lloyd SKW, Ramsden RT. Neurofibromatosis type 2. Adv Otorhinolaryngol 2011;70:91-8.

10. Coy S, Rashid R, Stemmer-Rachamimov A, Santagata S. An update on the CNS manifestations of neurofibromatosis type 2. Acta Neuropathol 2020;139:643-65.

11. Ota Y, Naganawa S, Kurokawa R, et al. Assessment of MR imaging and CT in differentiating hereditary and nonhereditary paragangliomas. AJNR Am J Neuroradiol 2021;42:1320-6.

12. Ota Y, Liao E, Capizzano AA, et al. Diagnostic role of diffusion-weighted and dynamic contrast-enhanced perfusion MR imaging in paragangliomas and schwannomas in the head and neck. AJNR Am J Neuroradiol 2021;42:1839-46.

13. Kleijwegt MC, van der Mey AG, Wiggers-deBruine FT, Malessy MJ, van Osch MJ. Perfusion magnetic resonance imaging provides additional information as compared to anatomical imaging for decision-making in vestibular schwannoma. Eur J Radiol Open 2016;3:127-33.

14. Zimny A, Sasiadek M. Contribution of perfusion-weighted magnetic resonance imaging in the differentiation of meningiomas and other extra-axial tumors: case reports and literature review. J Neurooncol 2011;103:777-83.

15. Ota Y, Liao E, Kurokawa R, et al. Diffusion-weighted and dynamic contrast-enhanced MRI to assess radiation therapy response for head and neck paragangliomas. J Neuroimaging 2021;31:1035-43.

16. Ota Y, Moore AG, Spector ME, et al. Prediction of wound failure in patients with head and neck cancer treated with free flap reconstruction: utility of CT perfusion and MR perfusion in the early postoperative period. AJNR Am J Neuroradiol 2022 [Epub ahead of print].

17. Sobel RA. Vestibular (acoustic) schwannomas: histologic features in neurofibromatosis 2 and in unilateral cases. J Neuropathol Exp Neurol 1993;52:106-13.

18. Ota Y, Liao E, Capizzano AA, et al. MR diffusion and dynamic-contrast enhanced imaging to distinguish meningioma, paraganglioma, and schwannoma in the cerebellopontine angle and jugular foramen. J Neuroimaging 2021 [Epub ahead of print].

19. Ota Y, Liao E, Capizzano AA, et al. Neurofibromatosis type 2 versus sporadic vestibular schwannoma: The utility of MR diffusion and dynamic contrast-enhanced imaging. J Neuroimaging 2022 [Epub ahead of print].

20. Welker K, Boxerman J, Kalnin A, et al. ASFNR recommendations for clinical performance of MR dynamic susceptibility contrast perfusion imaging of the brain. AJNR Am J Neuroradiol 2015;36:E41-51.

21. Schmainda KM, Prah MA, Rand SD, et al. Multisite concordance of DSC-MRI analysis for brain tumors: results of a national cancer institute quantitative imaging network collaborative project. AJNR Am J Neuroradiol 2018;39:1008-16.

22. Wang S, Martinez-Lage M, Sakai Y, et al. Differentiating tumor progression from pseudoprogression in patients with glioblastomas using diffusion tensor imaging and dynamic susceptibility contrast MRI. AJNR Am J Neuroradiol 2016;37:28-36.

23. Lewis D, Roncaroli F, Agushi E, et al. Inflammation and vascular permeability correlate with growth in sporadic vestibular schwannoma. Neuro Oncol 2019;21:314-25.

24. Gugel I, Zipfel J, Hartjen P, et al. Managing NF2-associated vestibular schwannomas in children and young adults: review of an institutional series regarding effects of surgery and bevacizumab on growth rates, tumor volume, and hearing quality. Childs Nerv Syst 2020 36:2471-80.

Tables

Table 1. Patient demographic and conventional imaging characteristics

	Paraganglioma	Sporadic schwannoma	NF2-related schwannoma
Number of patients	12	19	10
Sex (male/total)	6/12	12/19	1/10
Age (years)	31 (22-48)	50 (43-58)	21 (16-53)
Main location (CPA, JF, PC)	12 JF	11 CPA, 5 JF, 3 PC	8 CPA, 1 JF, 1PC

CPA, cerebellopontine angle; JF, jugular foramen; PC, prepontine cistern; values presented as the median (interquartile range).

Table 2 Conventional MRI imaging findings

	Paraganglioma	Sporadic schwannoma	NF2-related schwannoma	P-value
Number of patients	12	19	10	Not applicable

Maximum axial diameter (mm)	26 (23-38)	25 (17-34)	25 (20-30)	.93
Presence of cystic or necrotic change	9/12	12/19	7/10	.51
Enhancement pattern (homogeneous/total)	2/12	6/19	5/10	.27

Values are presented as the median (interquartile range).

Table 3 Comparisons of nADCmean, nrCBV, and nrCBF among intracranial paragangliomas, intracranial sporadic, and intracranial NF2-related schwannomas

					p value[b]		
	Paraganglioma	Sporadic schwannoma	NF2-related schwannomas	p value[a]	Paraganglioma vs sporadic schwannoma	Paraganglioma vs NF2-related schwannoma	Sporadic vs NF2-related schwannoma
nADCmean	1.48 (1.19-1.58)	1.58 (1.45–1.80)	1.23 (1.17–1.34)	<.001	p= .26	p= .29	p< .001
nrCBV	11.5 (6.24–13.6)	1.14 (0.94–1.35)	3.74 (2.86–4.84)	<.001	p< .001	p= .004	p< .001
nrCBF	7.43 (4.30–11.4)	1.13 (1.03–1.46)	2.85 (2.51–4.04)	<.001	p< .001	p= .007	p< .001

nADCmean, normalized mean apparent diffusion coefficient; nrCBV, normalized relative cerebral blood volume; nrCBF, normalized relative cerebral blood flow; P value[a] is based on Kruskal–Wallis H test. P value[b] is adjusted for pairwise comparison by Bonferroni correction.

Table 4. Inter-reader agreements for conventional imaging and quantitative analysis

Metrics	Reader 1 vs. Reader 2
Cystic/necrotic change	0.660
Enhancement pattern (homogeneous or heterogeneous)	0.609
nADCmean	0.923
nrCBV	0.950
nrCBF	0.934

Inter-reader agreements for conventional imaging findings were assessed by the kappa coefficient and for quantitative parameters was by intraclass correlation coefficient. nADCmean, normalized mean apparent diffusion coefficient; nrCBV, normalized relative cerebral blood volume; nrCBF, normalized relative cerebral blood flow

Figures

Figure 1

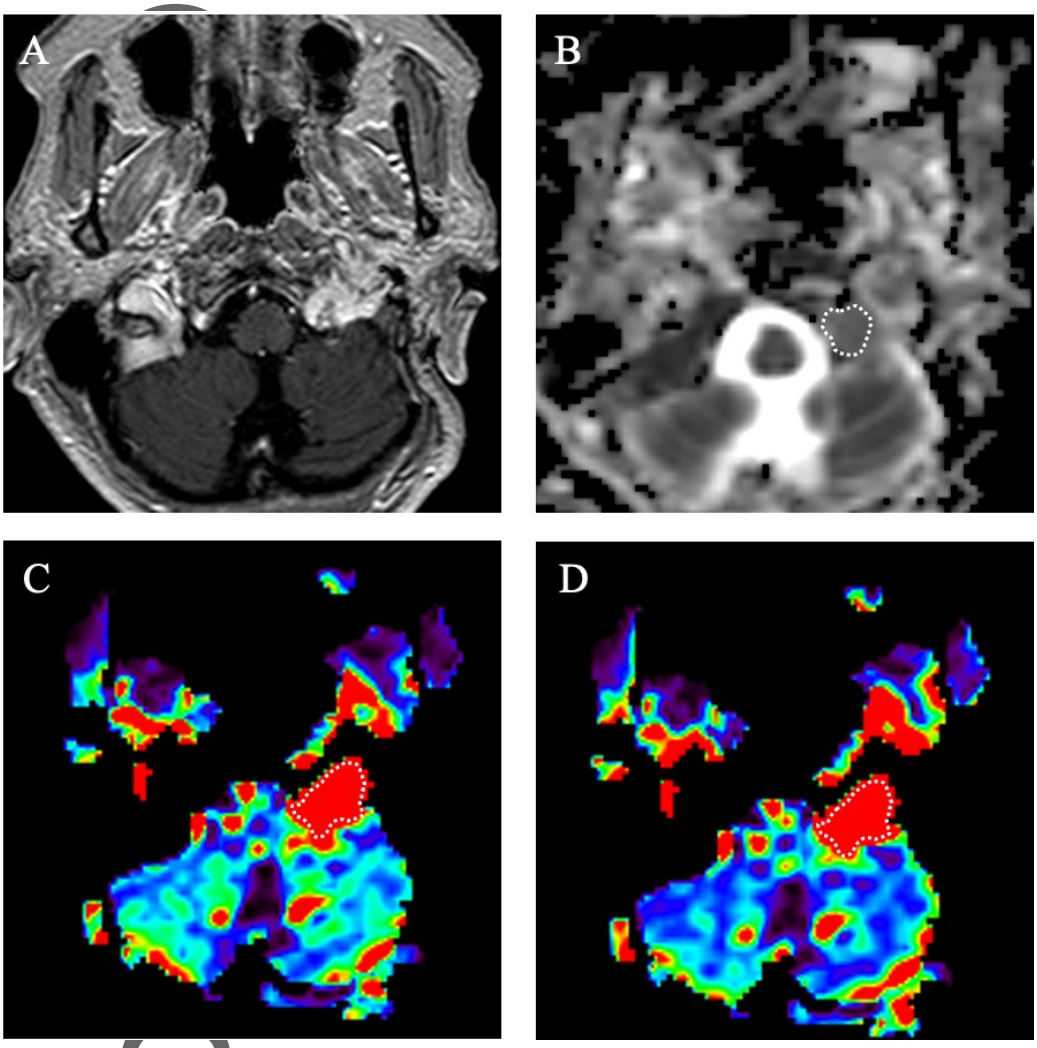

Fig1. A 67-year-old female with paraganglioma in the left jugular foramen.

(a) Post-contrast T1-weighted image shows a heterogeneously enhancing tumor in the left jugular foramen. (b) A region of interest was placed on the ADC map. The calculated normalized ADC mean was 1.35. (c) The rCBV and (d) rCBF were generated from DSC-MRI, and the corresponding nrCBV and nrCBF were 14.6 and 14.7, respectively.

nrCBV, normalized relative cerebral blood volume; nrCBF, normalized relative cerebral blood flow

Figure 2

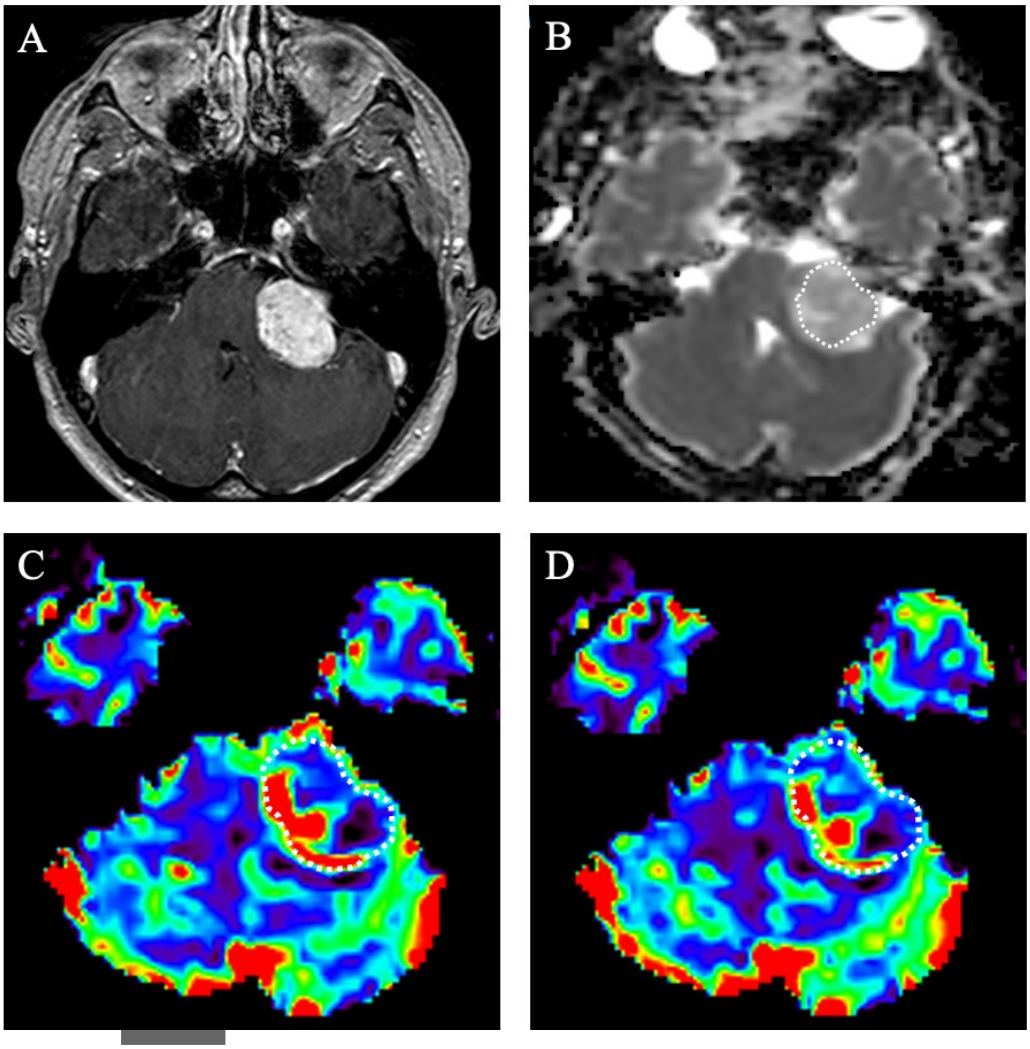

Fig 2. A 37-year-old-male with schwannoma in the left cerebellopontine angle.

(a) Post-contrast T1-weighted image shows a heterogeneously enhancing mass in the left cerebellopontine angle. (b) The ADC map was generated. The calculated normalized ADC mean is 1.62. (c) The rCBV and (d) rCBF were generated from DSC-MRI, and the calculated nrCBV and nrCBF were 0.85 and 1.02, respectively.

nrCBV, normalized relative cerebral blood volume; nrCBF, normalized relative cerebral blood flow

Figure 3

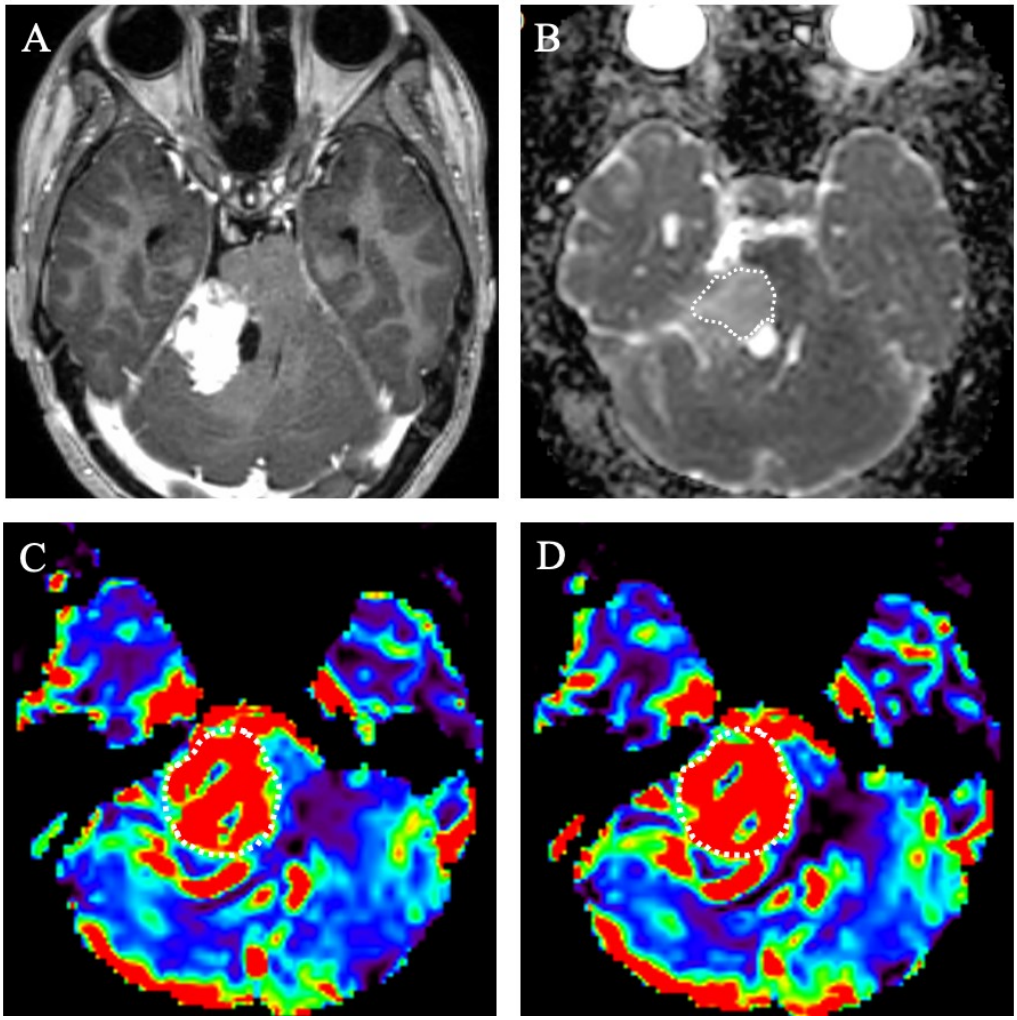

Fig. 3 A 18-year-old neurofibromatosis type 2 female with schwannoma in the right cerebellopontine angle.

(a) Post-contrast T1-weighted image shows a heterogeneously enhancing mass with a cystic component in the medial aspect, in the right cerebellopontine angle. (b) The ADC map was generated, and the calculated normalized ADC mean was 1.34. (c) The rCBV and (d) rCBF were generated from DSC-MRI, and calculated nrCBV and nrCBF were 5.05 and 5.83, respectively.

nrCBV, normalized relative cerebral blood volume; nrCBF, normalized relative cerebral blood flow

Figure 4

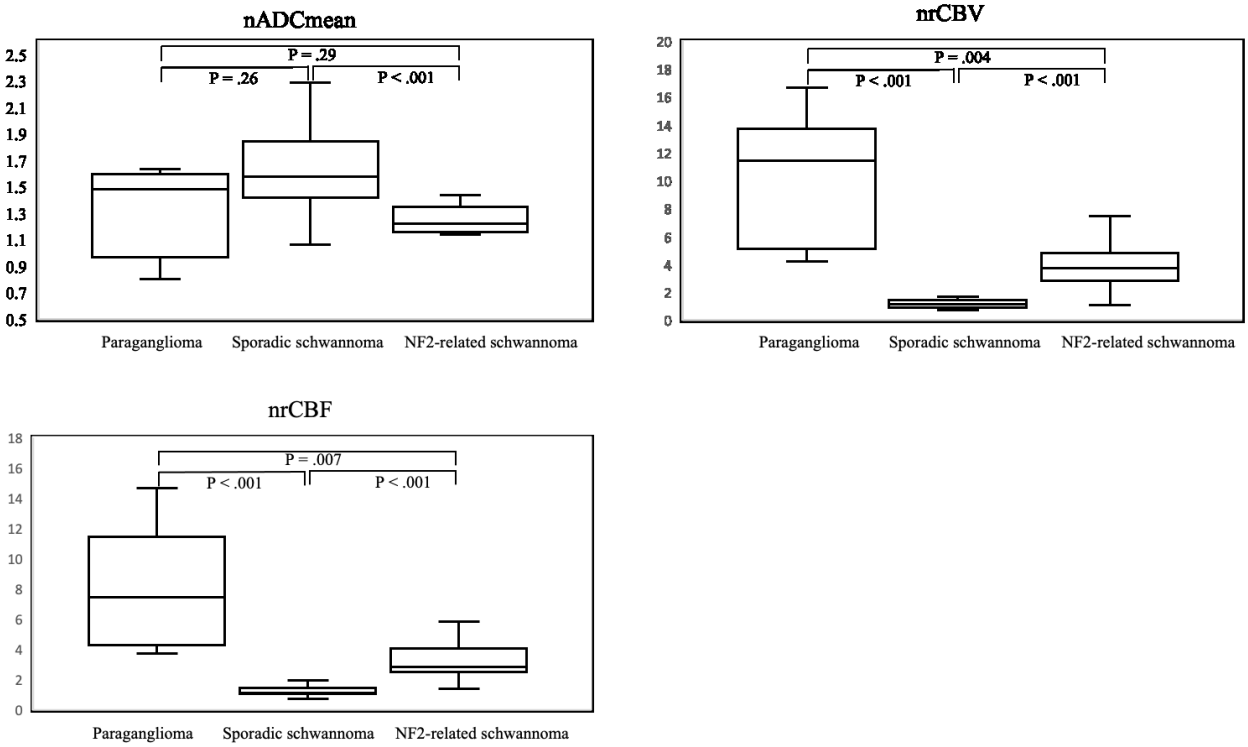

Fig.4 Box-and-whisker plots of nADC, nrCBV, and nrCBF with Kruskal–Wallis H test and post hoc test with Bonferroni correction are shown. Boundaries of boxes represent 25th and 75th percentiles, and lines in boxes indicate medians.

nADCmean, normalized mean apparent diffusion coefficient; nrCBV, normalized relative cerebral blood volume; nrCBF, normalized relative cerebral blood flow